Available online at www.pelagiaresearchlibrary.com

Pelagia Research Library

Advances in Applied Science Research, 2013, 4(4):91-98

ISSN: 0976-8610
CODEN (USA): AASRFC

Investigation of underground dam in coastal aquifers for prevention of saltwater intrusion

Mehdi Nezhad Naderi, Masoud Reza Hessami Kermani and Gholam-Abbas Barani

Department of Civil Engineering, Shahid Bahonar University, Kerman, Iran

---

ABSTRACT

Because of density difference between saltwater and freshwater is formed a transition zone between two fluids in coastal aquifers. Forward rate and extent of saltwater transition zone depends on several factors including: changes in sea level, aquifer characteristics, hydrological conditions of upstream, tidal and seasonal fluctuations of seawater. One of ways for prevention of seawater intrusion in coastal aquifer is construction of underground dam. In this paper, changes of hydraulic gradient in groundwater aquifer by *construction of underground dam is caused to reduce seawater intrusion to coast. The multiphase flow is simulated by computational fluid dynamics method.*

Keywords: underground dam, multiphase flow, computational fluid dynamic method, Prevention of seawater intrusion, Fluent Software.

INTRODUCTION

Fresh groundwater in the coastal aquifer is drained seas or lakes under natural conditions and the interface line between fresh and salt water occurs. Heavy exploitation of coastal aquifers has effect on the hydraulic gradient. Changes of hydraulic gradient in groundwater aquifer are caused advance of salt water far away the sea at the coast. This phenomenon is called seawater intrusion. Two researchers named Ghybn and Herzberg separately studied fresh underground water flow to the oceans along the coasts of Europe**.** They found that anywhere from a coastal aquifer, If depth of interface between fresh and saltwater is measured from sea level, (h_s), then level of fresh ground water from sea level, (h_f), will be 1/40 (h_s) in that point ([1]; [2]). Since these studies were started by two scientists this phenomenon is mentioned with regard to "Ghyben - Herzberg" that will be explained. Many reviews on the types of groundwater management models and their applications are made by [3], and [4]. The management models applications in saltwater intrusion, are relatively recent, [5], [6], [7], [8], [9], [10], [11], [12] and [13]. Perpendicular section is considered on the seaside in an aquifer (Fig. 1). Hydrostatic pressure at point A is:

$$P_A = \rho_s g h_s \quad (1)$$

That ρ_s is density of salt water, h_s is height of point A from sea level, and g is acceleration of gravity. Similarly, the hydrostatic pressure at point B that has the same depth to point A equals:

$$P_B = \rho_f g h_f + \rho_f g h_s \quad (2)$$

ρ_f is density of fresh water, h_f is freshwater height above sea level in the aquifer layer. Now, if the above two equations equal then Ghybn–Herzberg relationship would obtain as follows (see Fig (1), (2) and (3)):

$$h_s = \frac{\rho_f}{\rho_s - \rho_f} h_f \quad (3)$$

If in equation (3) the density of the salt water is 1.025 $\frac{g}{m^3}$ and fresh water density is 1 $\frac{g}{m^3}$ then equation (4) is calculated as follows:

$$h_s = 40 h_f \quad (4)$$

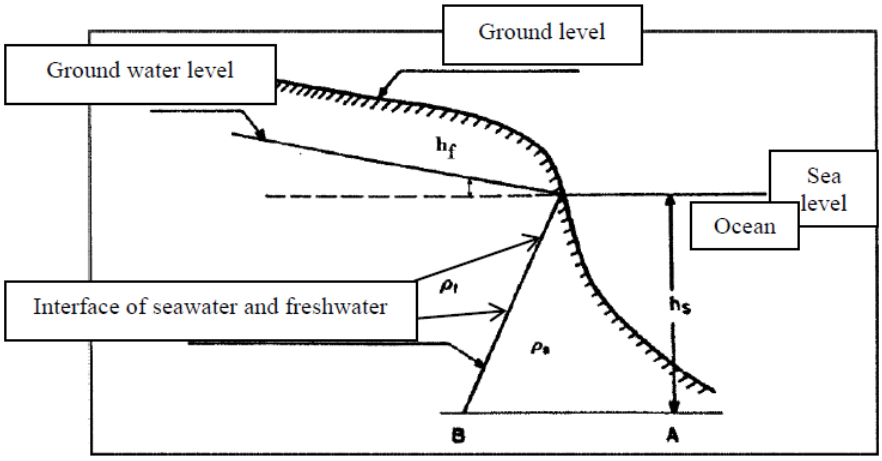

Fig (1). Ghyben – Herzberg relationship parameters

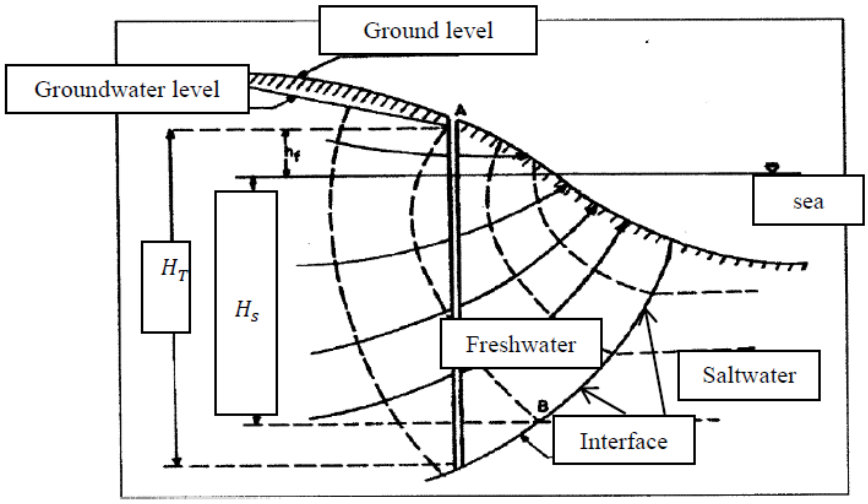

Fig (2). Ghyben – Herzberg relationship parameters

H_T is exact depth of interface and H_s is depth of interface based on Ghyben- Herzberg relationship that is lesser than H_T

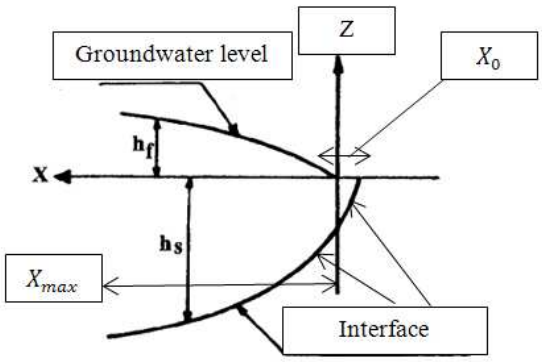

Fig (3). Ghyben – Herzberg relationship parameters

Thus it is seen that the influence of saline water into coastal freshwater aquifer depends on h_f the height of ground water level above the sea level. True picture of the quality of sea water intrusion are shown in Figure 2 by using flow lines and potential lines. [14] derived a single potential theory such that a single governing equation could be applies to both the saltwater and the freshwater zones. Figures 4(a) and (b) give a definition sketch in the vertical cross-section of a confined and an unconfined aquifer, respectively. Distinction has been made between two zones -a freshwater only zone (zone 1), and a freshwater-saltwater coexisting zone (zone 2). [14] demonstrated that for a homogeneous aquifer of constant thickness, a potential Φ which is continuous across the two zones, can be defined:

(a)

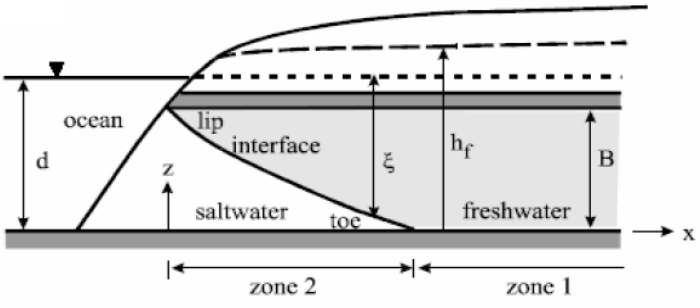

(b)

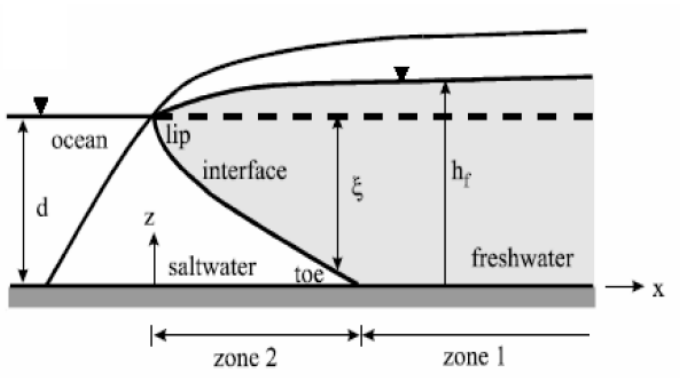

Fig (4). Definition sketch of saltwater intrusion in (a) a confined aquifer, and (b) an unconfined aquifer

In this study, flow is unsteady with two-dimensional turbulence form. Velocity and pressure are a function of time and space. To model of the velocity and pressure fluctuations is the integrated from the Navier Stokes equation at time. In this study, flow is steady with two-dimensional turbulence form. To model of the velocity and pressure fluctuations is the integrated from the Navier Stokes equation at time. Integration of Navier Stokes equations at time is known Reynolds equations [15]. Turbulence model equations are two equation models k-ε (Standard) that have be averaged in depth [16]. ε equation is as one of the main sources of the limitations of accuracy of the standard version of the k-ε model and the Reynolds stress model. It is interesting that k-ε model includes a correction term that is

dependent to strain with c13 constant in the ε equation of RNG model [17]. WillCox provided turbulence equations of k-ω (standard) model [18].

MATERIALS AND METHODS

$$\frac{\partial u}{\partial x}+\frac{\partial v}{\partial y}+\frac{\partial w}{\partial z}=0 \tag{5}$$

$$\frac{\partial \rho u}{\partial t}+\frac{\partial \rho uu}{\partial x}+\frac{\partial \rho uv}{\partial y}+\frac{\partial \rho uw}{\partial z}-\rho f_c v=-\frac{\partial P}{\partial x}+\frac{\partial \tau_{xx}}{\partial x}+\frac{\partial \tau_{xy}}{\partial y}+\frac{\partial \tau_{xz}}{\partial z} \tag{6}$$

$$\frac{\partial \rho v}{\partial t}+\frac{\partial \rho uv}{\partial x}+\frac{\partial \rho vv}{\partial y}+\frac{\partial \rho vw}{\partial z}+\rho f_c u=-\frac{\partial P}{\partial y}+\frac{\partial \tau_{yx}}{\partial x}+\frac{\partial \tau_{yy}}{\partial y}+\frac{\partial \tau_{yz}}{\partial z} \tag{7}$$

$$\frac{\partial \rho w}{\partial t}+\frac{\partial \rho uw}{\partial x}+\frac{\partial \rho vw}{\partial y}+\frac{\partial \rho ww}{\partial z}=-\frac{\partial P}{\partial z}+\frac{\partial \tau_{zx}}{\partial x}+\frac{\partial \tau_{zy}}{\partial y}+\frac{\partial \tau_{zz}}{\partial z}-\rho g \tag{8}$$

Known two-equation model of k-ε (Standard) are presented for averaged form in depth as follows [16] :

$$\frac{\partial hk}{\partial t}+\frac{\partial U_j hk}{\partial x_j}=\frac{\partial}{\partial x_j}[(\nu+\frac{\nu_t}{\sigma_k})h\frac{\partial k}{\partial x}]+hP_k+hP_{kv}-h\varepsilon \tag{9}$$

$$\frac{\partial h\varepsilon}{\partial t}+\frac{\partial U_j h\varepsilon}{\partial x_j}=\frac{\partial}{\partial x_j}[(\nu+\frac{\nu_t}{\sigma\varepsilon})h\frac{\partial \varepsilon}{\partial x}]+hc_{1\varepsilon}\frac{\varepsilon}{k}P_k+hP_{\varepsilon v}-hc_{2\varepsilon}\frac{\varepsilon^2}{k} \tag{10}$$

$$\nu_t=c_\mu\frac{k^2}{\varepsilon},P_k=2\nu_t S_{ij}.S_{ij} \tag{11}$$

$$P_{kv}=c_k\frac{k^2}{\varepsilon},c_k=\frac{1}{c_f^{1/2}},P_{\varepsilon v}=c_\varepsilon\frac{u_f^4}{h^2},c_\varepsilon=\frac{1}{\sqrt{e_*\sigma_t}}\frac{c_{2\varepsilon}c_\mu^{1/2}}{c_f^{3/4}},c_f=\frac{u_f^2}{u^2+v^2+w^2}=\frac{n^2g}{h^{1/3}} \tag{12}$$

$$c_\mu=0.09,c_{\varepsilon 1}=1.44,c_{\varepsilon 2}=1.92,\sigma_k=1.0,\sigma_\varepsilon=1.31$$

P_{kv} and P_{kv} are production terms as result of non-uniform distribution velocity in depth that is stronger near-bed. P_k is production term of turbulent kinetic energy averaged in depth as result of velocity gradients in the plan. ν_t is the vortex viscosity. Turbulence model is used for calculation of lateral flow into one channel and is achieved much better results in comparison with ν_t for fixed parameters of rotational flow [20]. c_f is the bed friction coefficient. σ_t is Schmidt number that shows relationship between turbulence viscosity and turbulent diffusion coefficient according to the following equation:

$$\varepsilon_d=\frac{\nu_t}{\sigma_t} \tag{13}$$

Amount of σ_t is considered 0.5 [21]. Although values of σ_t are 0.5 to 2 in variable references [22]. e_* is coefficient that gives turbulence diffusion coefficient in depth by following equation [21].

$$\varepsilon_d=e_*hu_f \tag{14}$$

Direct measurement of color broadcasting in the fixed-width channels offers 0.15 for e_*. Although Keller and Rodi achieved better solutions for the velocity and stress within the composite channels [21]. On the other hand Biglari and Sturm have been assumed e_* equaled to 0.3 to get the better answer within the composite channels [22].

MCGurik and Rodi have considered $\frac{1}{\sqrt{e_* \sigma_t}}$ equaled to 3.6 [20]. In ε equation of RNG model includes a correction term $c_{\varepsilon 1}$ that is constant strain-dependent [17]. For k-ε (RNG), we have:

$$\frac{\partial h\varepsilon}{\partial t}+\frac{\partial U_j h\varepsilon}{\partial x_j}=\frac{\partial}{\partial x_j}[(\nu+\frac{\nu_t}{\sigma\varepsilon})h\frac{\partial \varepsilon}{\partial x}]+hc_{1\varepsilon}^{*}\frac{\varepsilon}{k}P_k+hP_{\varepsilon\nu}-hc_{2\varepsilon}\frac{\varepsilon^2}{k} \tag{15}$$

$$c_\mu=0.0845, c_{1\varepsilon}^{*}=c_{1\varepsilon}-\frac{\eta(1-\frac{\eta}{\eta_0})}{1+\beta\eta^3}, c_{1\varepsilon}=1.68, \sigma_k=1.39, \beta=0.012, c_{1\varepsilon}=1.42, \tag{16}$$

$$\eta=(2E_{ij}.E_{ij})^{1/2}\frac{k}{\varepsilon}, \eta_0=4.377$$

Only constant β is adjustable, high levels of turbulent data are obtained near-wall. All other constants are calculated explicitly as part of the RNG process.

$$\frac{\partial hk}{\partial t}+\frac{\partial U_j hk}{\partial x_j}=\frac{\partial}{\partial x_j}[(\nu+\frac{\nu_t}{\sigma_k})h\frac{\partial k}{\partial x}]+P_k+P_b-h\varepsilon \tag{17}$$

$$\frac{\partial h\varepsilon}{\partial t}+\frac{\partial U_j h\varepsilon}{\partial x_j}=\frac{\partial}{\partial x_j}[(\nu+\frac{\nu_t}{\sigma\varepsilon})h\frac{\partial \varepsilon}{\partial x}]+hc_{1\varepsilon}\frac{\varepsilon}{k}P_k+hc_1S_\varepsilon-hc_2\frac{\varepsilon^2}{k+\sqrt{\nu\varepsilon}}+S_\varepsilon \tag{18}$$

$$c_1=Max[0.43,\frac{\eta}{\eta+s}], \eta=s\frac{k}{\varepsilon}, s=\sqrt{2s_{ij}s_{ij}}, \mu_t=hc_\mu\frac{k^2}{\varepsilon}, P_k=-\rho\overline{u_i^{'}u_j^{'}}\frac{\partial u_j}{\partial x_i^{'}},$$

$$P_k=\mu_t s^2, P_b=\beta g_i\frac{\mu_t}{\mathrm{Pr}_t}\frac{\partial T}{\partial x_i}, \mu_t=\rho c_\mu\frac{k^2}{\varepsilon}, c_\mu=\frac{1}{A_0+A_s\frac{KU^*}{\varepsilon}}, U^*=\sqrt{s_{ij}s_{ij}+\overline{\Omega_{ij}}\,\overline{\Omega_{ij}}}, \tag{19}$$

$$\overline{\Omega_{ij}}=\Omega_{ij}-\varepsilon_{ijk}\omega_k, A_0=4.04, A_s=\sqrt{6}\cos\Phi, \Phi=\frac{1}{3}\cos^{-1}(\sqrt{6}\omega), \omega=\frac{s_{ij}s_{jk}s_{ki}}{\tilde{s}^3}, \tilde{s}=\sqrt{s_{ij}s_{ij}},$$

$$s_{ij}=\frac{1}{2}(\frac{\partial u_j}{\partial x_i}+\frac{\partial u_i}{\partial x_j}), c_{1\varepsilon}=1.44, c_2=1.9, \sigma_k=1, \sigma_\varepsilon=1.2, \beta=-\frac{1}{\rho}(\frac{\partial P}{\partial T})p, \mathrm{Pr}_t=0.85$$

WillCox, turbulence model k-ω (standard) equation to be provided as follows [19]:

$$\frac{\partial k}{\partial t}+U_j\frac{\partial k}{\partial x_j}=\tau_{ij}\frac{\partial U_i}{\partial x_j}-\beta^{*}k\omega+\frac{\partial}{\partial x_j}[(\nu+\sigma^{*}\nu_T)\frac{\partial k}{\partial x_j}] \tag{20}$$

$$\frac{\partial \omega}{\partial t}+U_j\frac{\partial \omega}{\partial x_j}=\alpha\frac{\omega}{k}\tau_{ij}\frac{\partial U_i}{\partial x_j}-\beta\omega^2k\omega+\frac{\partial}{\partial x_j}[(\nu+\sigma\nu_T)\frac{\partial \omega}{\partial x_j}] \tag{21}$$

$$\nu_t=\frac{k}{\omega}, \alpha=\frac{5}{9}, \beta=\frac{3}{40}, \beta^{*}=\frac{9}{100}, \sigma=\frac{1}{2}, \varepsilon=\beta^{*}\omega k$$

The values of the physical properties of water are considered 998.2, 0.001003, 4182 and 0.6, respectively, for density, viscosity, heat capacity and thermal conductivity. Solutions of all governing equations are subject to assignment of variables correctly in the boundary nodes. In steady state problems required only boundary condition but in unsteady state problems is required the initial conditions for all nodes in the network. Common boundary conditions in hydraulic issues include [23]:

A- Inlet boundary condition: numerical models can fit the model by means of the various boundary conditions such as velocity, mass flow, etc. For example, in modeling of flow inside a closed or open channel can be used velocity inlet as input boundary condition. B- The outlet boundary condition is considered pressure outlet equals the atmospheric pressure. If the output is chosen at a far distance from geometric constraints, and no change in direction of flow then the flow state is developed full. Using this model is caused the output surface is perpendicular to the flow and gradient is zero in the perpendicular direction on the output surface [23]. C - Wall boundary condition: the wall boundary condition is used to limit the area of between fluid and solid. The model is ready for simulation by Solutions set and defining the model. The following steps show the simulation process [24]: selection methods of discretization equation: In this paper first order upstream difference method is used for discretization of momentum, k, ε and ω equations and the standard method is used to find the pressure. Selection methods of the relation velocity - Pressure: this step is only be studied segregated. In this paper is used from SIMPLE method for velocity - pressure coupling. Determine the discount factors: the discount factor values are used for control of calculated variables in the each iteration. In this paper, the default values 0.3, 1, 0.7, 0.8, 0.8 and 1 is used respectively for the pressure, density, momentum, k, ε and turbulent viscosity. In this paper, the initial values of the relative pressure is considered zero And the initial values of velocity components close to the average values presented in the input stream. By completing the steps in the numerical model, we can start the introduced process of problem by defining of repeat process. The frequency of reporting of results can be introduced before computing the numerical model. During solution process can be seen convergence of solution by the control of residues, integral of surface, statistics and values of the force. After finishing solution the computation of the unknown quantities and the results can be calculated at any point of the field and can be displayed by vector in the form, contour and profile [24]. In this paper for solution of flow is usually introduced initial number repeat 1000 with report of every step of the calculation that conditions for convergence of the unknown parameters were satisfied after 300 to 350 iterations. Gambit software version 2.3.16 is used to generate the channel geometry and meshing [25]. Model of the network is used Quad element and the types of Map and Pave for pages and Hex elements and types of Map of Cooper for volumes. Inlet and outlet and wall boundary conditions and symmetry were introduced in the software.

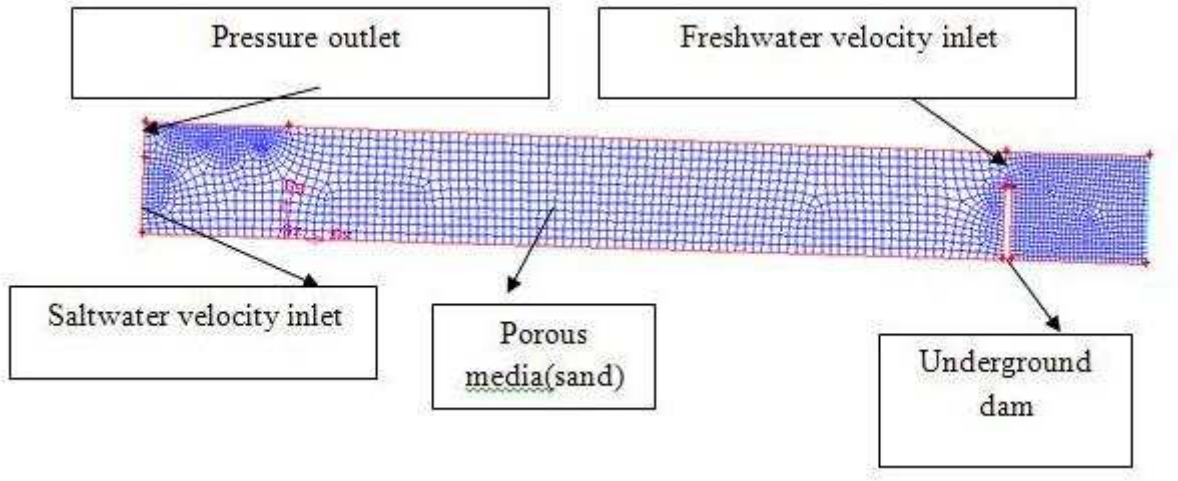

Fig(5). Meshing model in Gambit software

RESULTS AND DISCUSSION

Gambit software version 2.3.16 is used to generate the channel geometry and meshing. Model of the network is used Quad element and the types of Map and Pave for pages and Hex elements and types of Map of Cooper for volumes. Inlet and outlet and wall boundary conditions and symmetry were introduced in the software. Saltwater inlet velocity is considered 1.157e-07 meters per second and Freshwater inlet velocity is considered to 0.05 meters per second. The results of the numerical models show that increasing freshwater hydraulic gradient and times are caused to reduce seawater intrusion to coast as figure 6-a to 6-c.

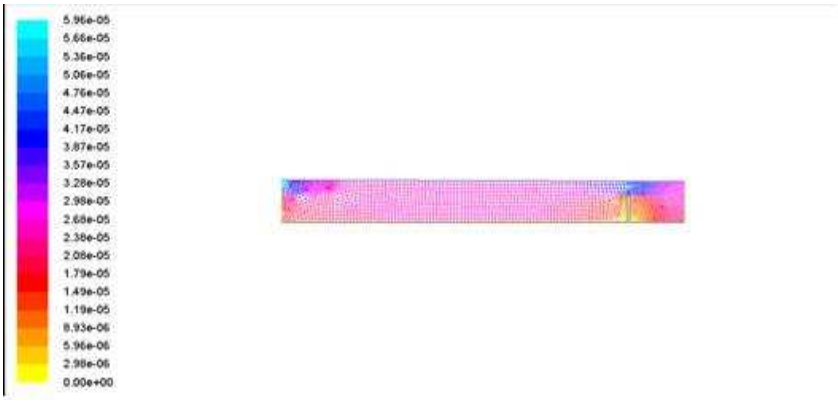

Fig(6).a. Velocity magnitude contours for the two phase flow for seawater intrusion from left input, freshwater from right input (time =1s)

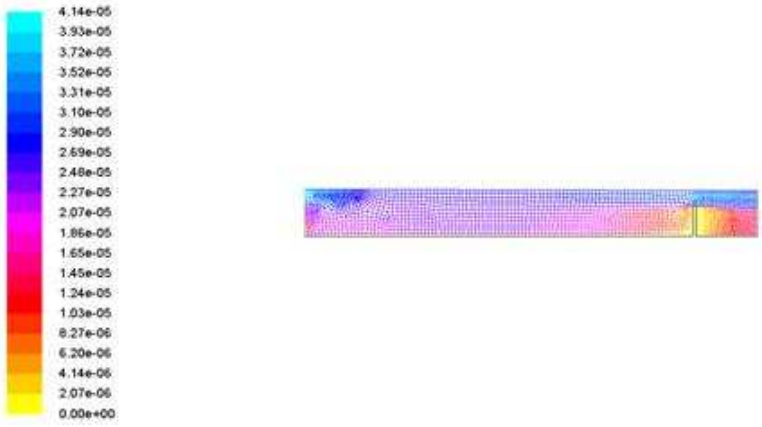

Fig(6).b. Velocity magnitude contours for the two phase flow for seawater intrusion from left input, freshwater from right input (time =6s)

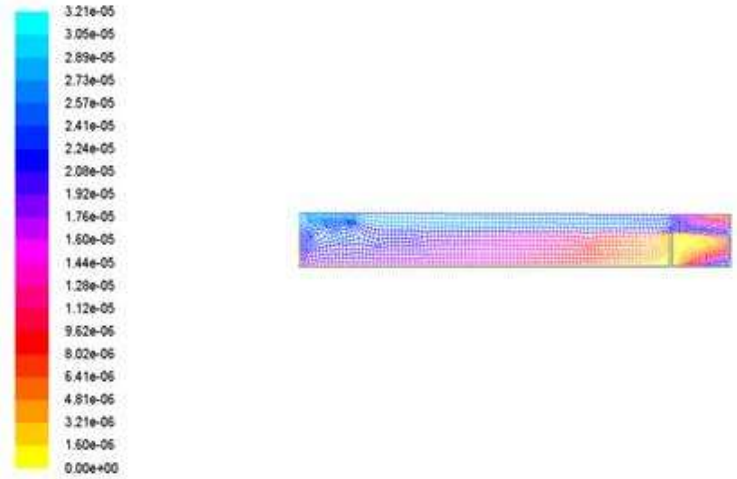

Fig(6).c. Velocity magnitude contours for the two phase flow for seawater intrusion from left input, freshwater from right input (time =46s)

CONCLUSION

The multiphase flow is simulated by computational fluid dynamics method in a coastal aquifer. In this paper is paid to two-phase flow simulation by software Fluent6.3 that freshwater input is from the left side and saltwater input is on the right side over underground dam. By using of mixture model and k-ε turbulence model in software the two-phase mixture is dissolved. Saltwater inlet velocity is considered 1.157e-07 meters per second and Freshwater inlet velocity is considered to 0.05 meters per second. The results of the numerical models show that increasing freshwater hydraulic gradient by construction of underground dam is caused to reduce seawater intrusion to coast.

REFERENCES

[1] GHYBEN, W. B., **1889**. Nota in Verband Met de Woorgenomen Putboring Nabij Amesterdam. Tijdschrift van Let Koninklijk Inst. Van Ing.
[2] Herzberg, B., **1992**. *Jour. Gasbeleuchtung and Wasserversorgung*, V. 44, pp. 815- 819, 842-884- Mumich.
[3] Gorelick, S.M., **1983**. *Water Resour. Res.*, 19, 305-319.
[4] Yeh, W.W.-G, **1986**. *Water Resour. Res.*, 22, 95-108.
[5] Cheng, A.H.-D., Halhal, D., Naji, A. and Ouazar, D., **1999**. Pumping Optimization in Saltwater – intruded Coastal Aquifers, *J. Water Resourc*. Research, submitted.
[6] Fatemi, E., Ataie-Ashtiani., **2008**. Simulation of Seawater Intrusion Effect on Contaminant transport in coastal aquifer of Tallar, 4th National Congress of Civil Engineering, Tehran university in Iran.
[7] Bear, J. and Cheng, A.H.-D., **1999**. An overview, Chap. 1, In Seawater Intrusion in Coastal Aquifers---Concepts, Methods, and Practices, eds. J. Bear, A.H.-D. Cheng, S. Sorek D. Ouazar and I. Herrera, Kluwer, 1-8.
[8] Cheng, A.H.-D., Ouazar, D., **1999**. Analytical solutions," Chap. 6, "Seawater Intrusion in Coastal Aquifers---Concepts, Methods, and Practices", eds. J. Bear, A.H.-D. Cheng, S. Sorek D. Ouazar and I. Herrera, Kluwer, 163-191.
[9] Cummings, R.G., **1971**. *J. Water Resources Research*, Vol 7, N° 6, 1415-1424.
[10] Cummings, R.G. and McFarland, J. W., **1974**. *J. Water Resources Research*, Vol 10, N° 5, 909-915.
[11] Dagan, G. and Bear, J. **1968**. *J. Hydrol. Res*., v. 6, p. 15-44.
[12] Das Gupta, A., Nobi, N and Paudyal G.N., **1996**. *J. Ground Water*, vol 34, N°2, 349-357.
[13] Naji, A., Cheng, A.H.-D. and Ouazar, D., **1999**. *Eng. Analy. Boundary Elements*, 23, 529-537.
[14] Strack, O.D.L., **1976**. *Water Resour. Res.*, 12, 1165-1174.
[15] Reynolds, O. **1984**. On the Dynamical Theory of Incompressible Viscous Fluids and the Determination of the Criterion, Phil. Trans. Roy. Soc. London, **1986**, 123-161.
[16] Rastogi, A. K., and Rodi, W. **1978**. *Journal of Hydraulics Division*, ASCE, 104(3), 397- 420.
[17] Yakhot, V., Orszag, S.A., Thangam, S., Gatski, T. B., and speziale, C. G. **1992**. *Physics of Fluids* A, Vol. 4, No. 7, pp1510-1520.
[18] Wilcox, D. C. **1988**. *AIAA Journal*, vol. 26, pp. 1414- 1421.
[19]McGurik, J. J., and Rodi, W. **1978**. *Journal of Fluid Mechanics*, 864, 761-781.
[20]Keller, R. J., and Rodi, W. **1988**. *Journal of Hydraulic Research*, IAHR, 26(4), 425-441.
[21] Gibson, M. M., and Launder, B. E. **1978**. *Journal of Fluid Mechanics*, 86, 491-511.
[22] Biglari, B., and Sturm, T. W. **1998**. *Journal of Hydraulic Engineering*, ASCE, 124(2), 156-163.
[23] Soltani, M. V. and Rahimi Asl,R., **2003**. Computational Fluid Dynamics by Fluent Software, Tehran, Tarrah issues.
[24] Versteeg, H. K. and Malalasekera, W. **1995**. An Introduction to Computational Fluid Dynamics.
[25] GAMBIT 2.2 User's Guide, September **2004**.